ACS NANO

www.acsnano.org

ARTICLE

Ultrasensitive and Specific Clustered Regularly Interspaced Short Palindromic Repeats Empowered a Plasmonic Fiber Tip System for Amplification-Free Monkeypox Virus Detection and Genotyping

Yuzhi Chen,[#] Zhi Chen,[#] Tianzhong Li, Meng Qiu, Jinghan Zhang, Yan Wang, Wu Yuan, Aaron Ho-Pui Ho, Omar Al-Hartomy, Swelm Wageh, Abdullah G. Al-Sehemi, Xin Shi, Jingfeng Li,* Zhongjian Xie,* Li Xuejin,* and Han Zhang*

Cite This: *ACS Nano* 2023, 17, 12903−12914

Read Online

ACCESS | Metrics & More | Article Recommendations | Supporting Information

ABSTRACT: **The urgent necessity for highly sensitive diagnostic tools has been accentuated by the ongoing mpox (monkeypox) virus pandemic due to the complexity in identifying asymptomatic and presymptomatic carriers. Traditional polymerase chain reaction-based tests, despite their effectiveness, are hampered by limited specificity, expensive and bulky equipment, labor-intensive operations, and time-consuming procedures. In this study, we present a clustered regularly interspaced short palindromic repeats (CRISPR)/Cas12a-based diagnostic platform with a surface plasmon resonance-based fiber tip (CRISPR-SPR-FT) biosensor. The compact CRISPR-SPR-FT biosensor, with a 125 μm diameter, offers high stability and portability, enabling exceptional specificity for mpox diagnosis and precise identification of samples with a fatal mutation site (L108F) in the *F8L* gene. The CRISPR-SPR-FT system can analyze viral double-stranded DNA from mpox virus without amplification in under 1.5 h with a limit of detection below 5 aM in plasmids and about 59.5 copies/μL when in pseudovirus-spiked blood samples. Our CRISPR-SPR-FT biosensor thus offers fast, sensitive, portable, and accurate target nucleic acid sequence detection.**

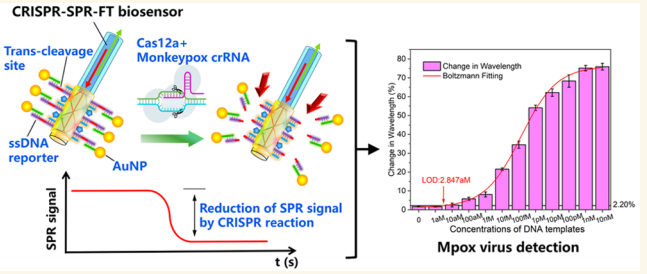

KEYWORDS: *Biosensor, Amplification-free, Surface plasmon resonance-based fiber tip, Clustered regularly interspaced short palindromic repeats (CRISPR), Monkeypox virus*

INTRODUCTION

Since the documented case of the mpox (previously known as monkeypox) virus (MPXV) in 1970, the number of MPXV outbreaks has steadily increased, primarily restricted to the African continent.[1] As of May 18, 2022, thousands of cases related to MPXV were reported within two months across over 30 countries, indicating a rapid global outbreak of MPXV in 2022.[2] Genetic distance analyses and clinical differences revealed two main clades of MPXV: Clade I, prevalent in the Congo Basin or Central Africa, and Clade II, predominant in West Africa.[3] However, following the third outbreak in 2003, the ongoing outbreak of MPXV produced a third clade (Clade III) with recently classified lineages: A.1, A.1.1, A.2, and B.1. All MPXV genomes isolated from the 2022 outbreak belong to lineage B.1.[4] Characteristic clinical manifestations of this recent outbreak include an initial genital or perianal rash, suggesting close physical contact as the primary transmission route.[5]

Due to the relatively low level of MPXV in the blood and body fluids,[6] MPXV infection is typically detected through polymerase chain reaction (PCR) testing of skin lesion samples. Traditional PCR testing, however, cannot directly detect specific mutations, such as the L108F substitution in the N-terminal

Received: June 4, 2023
Accepted: June 27, 2023
Published: June 29, 2023

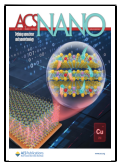

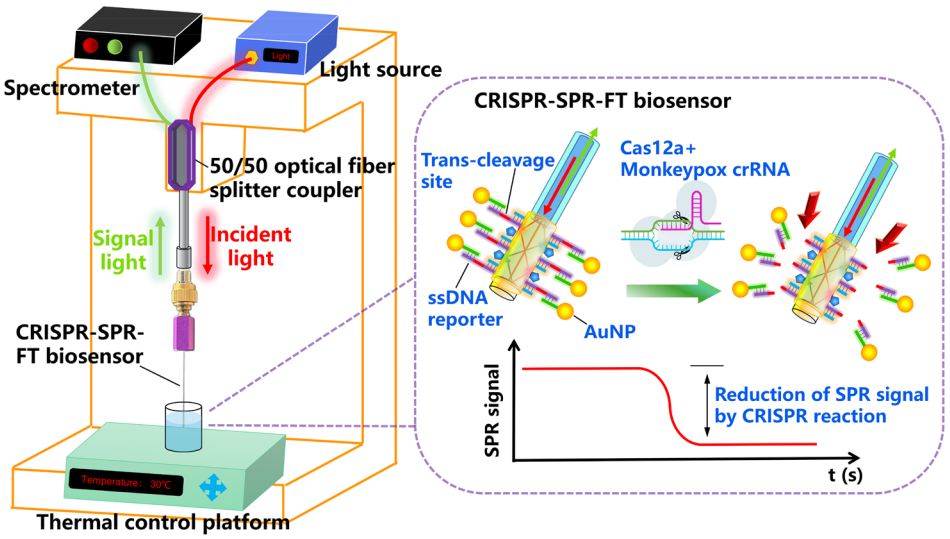

Figure 1. Schematic of the design of the portable CRISPR-SPR-FT biosensing platform for MPXV detection. The proposed CRISPR-SPR-FT biosensor was decorated with AuNPs through partial complementary DNAs, wherein ssDNA reporters with key trans-cleavage sites were designed on the biosensor. Target DNA activates Cas12a−crRNA, causing the trans-cleavage of ssDNA reporters. During CRISPR/Cas12a sensing, the spectral signal is transmitted and recorded in real-time through a fiber-based biosensing system. The loss of AuNPs on the sensor surface causes the corresponding changes in the SPR signal.

domain of the MPXV *F8L* gene, a gain-of-function mutation proposed to be related to enhanced processivity, lower sensitivity to nucleoside inhibitors, and fidelity of DNA synthesis.[7] Additionally, PCR and other amplification-dependent techniques are costly, laborious, and time-consuming and require skilled operators and expensive equipment. Consequently, there is an urgent need for gene-targeting platforms that are affordable and systematic, facilitating rapid and accurate MPXV detection.

The clustered regularly interspaced short palindromic repeats (CRISPR)-Cas system has been extensively applied as a revolutionary gene-editing technique.[8] Upon activation, two CRISPR/Cas nucleases, Cas12 and Cas13, display multiple-turnover trans-cleavage activity.[9,10] The Cas12a-clustered, regularly interspaced, short palindromic repeats RNA (crRNA) complex can be activated by double-stranded DNA (dsDNA) with the desired gene sequence and generate corresponding fluorescence signals by trans-cleaving unspecific single-stranded DNA (ssDNA) fluorescence-quencher reporters,[11−13] while Cas13a targets RNAs and trans-cleaves nonspecific ssRNA reporters.[14,15] Although several CRISPR-based diagnostic methods for mpox viruses have been developed, the prerequisite amplification steps limit their practical use[16−18] because amplification steps may produce nonspecific amplicons, prolong the detection time, raise the risk of carryover contamination, and limit the portability and integration of CRISPR-based detection devices. Since recent works about the CRISPR Cas12a-based POCT strategy have rapidly developed, like the gas reaction with a wireless sensor,[19] and the photoelectrochemical biosensing system using a hollow In_2O_3−In_2S_3-modified screen-printed electrode,[20] the feasibility of the CRISPR-based POCT strategy has been proven. Previously, we developed MoPCS (Methodologies of Photonic CRISPR Sensing), a low-cost CRISPR/Cas12a system-empowered surface plasmon resonance (SPR) gene-detecting platform, to analyze SARS-CoV-2 variants.[21] SPR-sensing technology is a versatile technique widely used in designing optical sensing platforms[22,23] and extensively employed in molecular interaction research, including antigen−antibody,[24] drug−target,[25] protein−nucleic acid,[26] protein−protein,[27] and protein−lipid[28] interactions, by monitoring the refractive index change on the sensor surface caused by the surface load changes. Our group has consistently focused on developing SPR-sensing technologies for specific nucleic acid-sensing applications.[29] Recently, we combined the CRISPR/Cas system with SPR to establish a CRISPR-empowered SPR diagnostic platform.[21,30] However, the CRISPR-empowered SPR platform prototype required bulky equipment and laborious procedures, making it insufficient for DNA/RNA diagnosis during a pandemic of infectious pathogens, such as MPXV and SARS-CoV-2.

Optical fiber SPR biosensors excel at immunodetection in liquid-phase environments by sensing changes in the surface load. Recently, Hua et al.[31] reported a DNA aptamer-decorated fiber SPR biosensor for the specific measurement of inflammation biomarkers, achieving a limit of detection (LOD) of 2.5 and 1.7 nM to cardiac troponin I and C-reactive protein, respectively. We also previously developed an SPR-based fiber biosensor to detect urine glucose samples via an enzymatic reaction performed by a self-made glucose decomposition device, obtaining a broad detection range of 0−400 mg/dL.[32] Similarly, the highly specific CRISPR/Cas12a method can identify target viral DNA, and the trans-cleavage mechanism of ssDNA reporters on an SPR fiber tip biosensor can induce surface load variations, demonstrating the feasibility of the principle.

Therefore, to address the limitations of the CRISPR-empowered SPR platform, we incorporated a miniaturized and portable SPR-based fiber tip biosensing system into the CRISPR/Cas12a-based diagnostic platform to achieve the rapid and portable detection of MPXV. The core CRISPR/Cas12a-based SPR fiber tip (CRISPR-SPR-FT) biosensor, with a tiny diameter of only 125 μm, was designed for single use,[33,34] offering the potential for large-scale, high-throughput detection. In this study, we first evaluated the performance of the biosensor in detecting surface load and temperature changes. We further assessed the LOD, specificity, and sensitivity of the CRISPR/

https://doi.org/10.1021/acsnano.3c05007
ACS Nano 2023, 17, 12903−12914

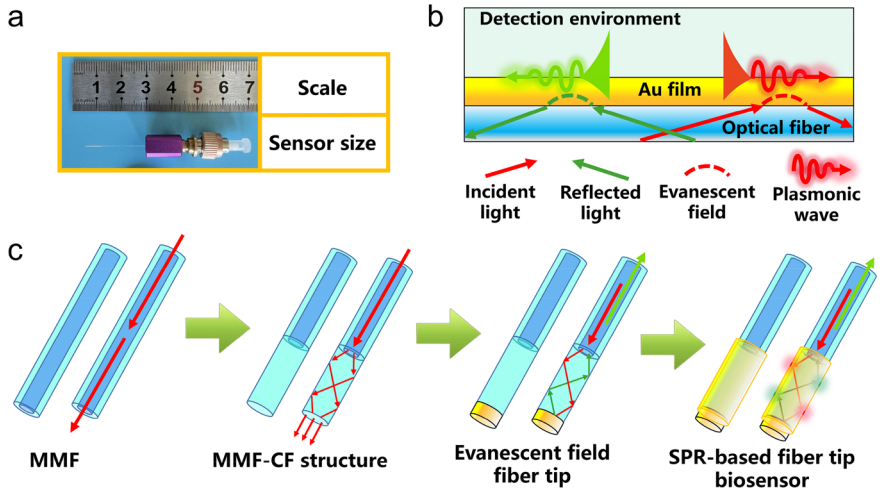

Figure 2. Disposable surface plasmon resonance (SPR)-based fiber tip biosensor. (a) Photograph of the 125 μm fiber tip biosensor. (b) SPR stimulation was on the sensor surface. (c) Engineering process of the proposed biosensor. MMF, multimodal fiber; CF, coreless fiber.

Cas12a fluorescence assay for comparison with our method. Lastly, we conducted on-device measurements in both plasmids and pseudovirus-spiked blood samples. The key advantages of the CRISPR-SPR-FT biosensing platform for accurate detection of MPXV include: (1) high sensitivity for amplification-free sample detection (LOD: < 5 aM); (2) the ability to distinguish the specific L108F mutation site in MPXV; (3) portability, thereby meeting the needs for large-scale point-of-care tests. Overall, this CRISPR-empowered biosensor facilitates precise, stable, sensitive, and reliable gene analysis of the MPXV.

RESULTS AND DISCUSSION

MPXV Detection Scheme Based on CRISPR-SPR-FT Sensing. The compact SPR-based fiber tip biosensor can sense a change in the surface load with ultrasensitivity.[35,36] Furthermore, the CRISPR/Cas12a system can recognize target DNA with high specificity and activate the trans-cleavage mechanism for ssDNA reporters. By designing ssDNA reporters on an SPR-based fiber tip biosensor, we combined these two technologies and proposed a CRISPR-SPR-FT biosensing platform for the portable detection of target DNA. Figure 1 illustrates the platform's principle for detecting target MPXV DNA. We designed a CRISPR-SPR-FT biosensor adorned with gold nanoparticles (AuNPs) via a pair of partially complementary DNAs containing an ssDNA reporter. In the presence of MPXV DNA, the CRISPR/Cas12a system could trans-cleave ssDNA reporters to release the AuNPs, resulting in a reduced surface load on the sensor surface and a subsequent decrease in the SPR signal.[37,38]

Disposable SPR-Based Fiber Tip Biosensor. Figure 2a displays a physical image of a disposable SPR-based fiber tip biosensor. A plug-in fiber tip with 125 μm diameter was deemed suitable for trace sample detection in a confined space. We utilized a disposable biosensor to prevent cross-contamination and ensure safety for viral detection. The biosensor was excited using broadband visible light.[39] Due to the end-face Au mirror on the outgoing end of the sensing fiber, the signal light was reflected, stimulating secondary SPR sensing in the sensing fiber. The signal was eventually received by the microspectrometer. A 50/50 optical fiber splitter coupler was employed to separate the incident and reflected light signals. A thermal control platform was used to adjust the temperature of the CRISPR/Cas12a process (Figure 1).

Figure 2b illustrates the sensing principle of the proposed biosensor's surface. SPR sensing was stimulated by evanescent fields resulting from the total reflections of the incident and reflected light.[40] Due to the end-face reflection of the Au mirror, the SPR sensing efficiency was doubled, leading to a halving of the sensing length, which further improves the biosensor's practicality.

Figure 2c demonstrates the engineering process of the SPR-based fiber tip biosensor. Since the transmission optical fiber cannot deliver light to the fiber surface, a hybrid fiber structure of multimode fibers (MMFs) and coreless fibers (CFs) was fabricated to stimulate the evanescent field on the CF surface. However, the signal light would be emitted from the outgoing end of the CF. To reflect the signal light, an end-face mirror was deposited on the outgoing end of the CF. Finally, the Au-sensing film was deposited on the CF cylindrical surface for SPR sensing.

Performance of the SPR-Based Fiber Tip Biosensor. A series of liquids with increasing refractive indices were prepared for surface load increase measurements. Due to the specific surface area of the fiber-sensing region, variations in the surface load could be reflected by changes in the liquid density, which in this case, are equivalent to changes in the refractive index (Figure 3a). The sensing signal (i.e., the SPR peak) exhibited an increased resonance wavelength shift (ΔRW) when the increasing refractive index was detected (Figure 3b). The refractive index gradient measurement results indicated that ΔRW was proportional to the change in the surface load (Figure 3c) with high stability and sensitivity. Specifically, the detection stability, measured by the average standard deviation ($\bar{\sigma}$), was 0.14 nm (Figure 3d), and the average sensitivity ($\bar{S}$) was 2276.50 nm/RIU (Figure 3e).

We further evaluated the temperature response of the proposed biosensor (Figure 3f). The SPR peak exhibited a decrease in the ΔRW with increasing temperature (Figure 3g). The temperature gradient measurement results indicated that ΔRW was inversely proportional to the change in temperature (Figure 3h) with a $\bar{\sigma}$ of 0.10 nm (Figure 3i) and $\bar{S}$ of −0.296 nm/°C (Figure 3j).

CRISPR/Cas12a Fluorescence Assay. To test the performance of the biosensor in MPXV detection, plasmids containing the F2L gene sequence of MPXV and similar sequences from

https://doi.org/10.1021/acsnano.3c05007
ACS Nano 2023, 17, 12903−12914

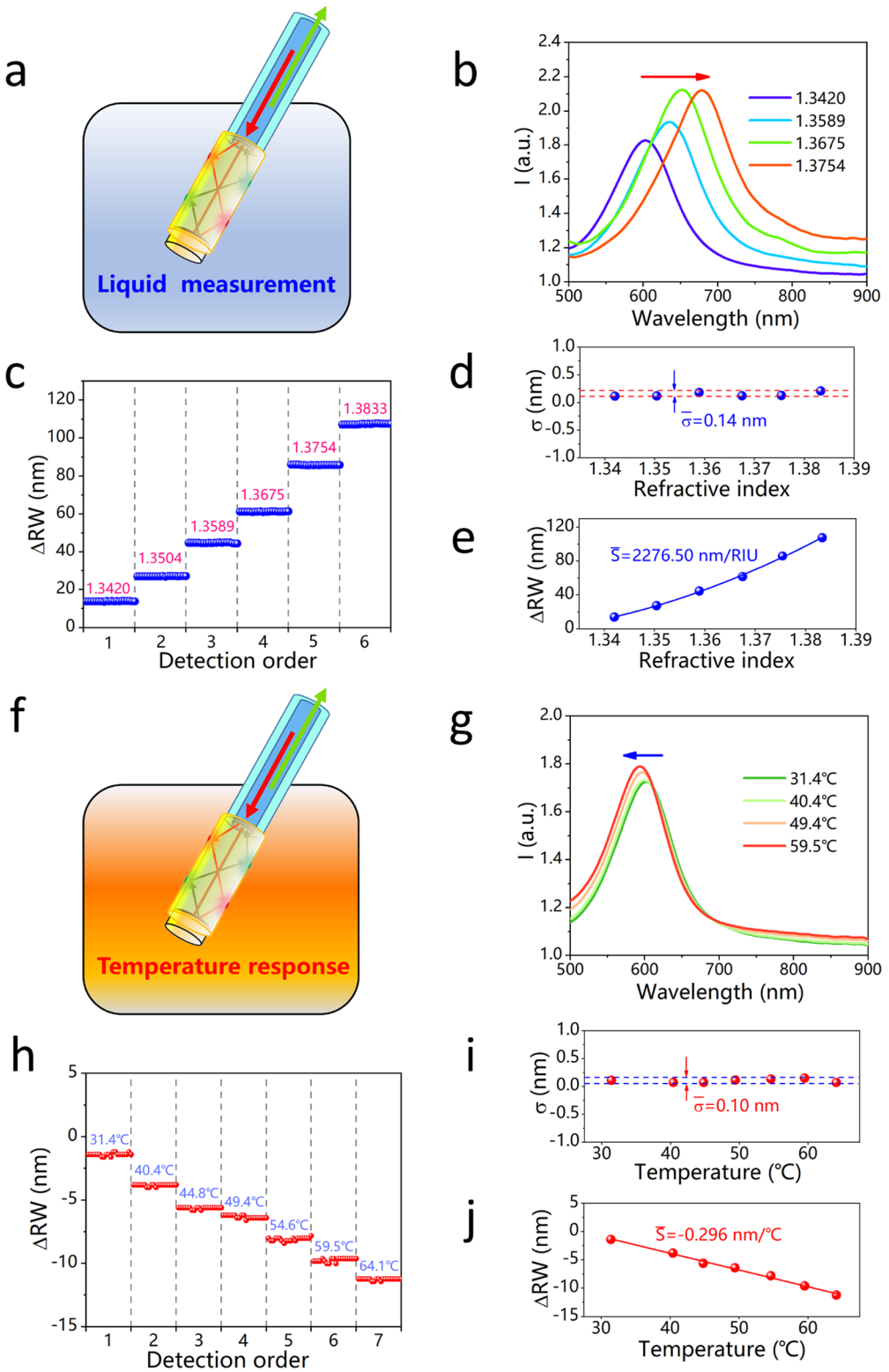

Figure 3. Sensor performance. (a) Diagram of the liquid measurement device. (b) Surface plasmon resonance (SPR) peak shifts in measuring the increasing refractive index. (c) Reading of the resonance wavelength shift (ΔRW) in liquid environments with different refractive indices. Each continuous measurement lasted 1 min. (d) Detection stability, calculated as the average standard deviation ($\bar{\sigma}$), and (e) average sensitivity ($\bar{S}$) were calculated using data from (c). (f) Diagram of the temperature response measurement device. (g) SPR peak shifts in measuring increasing temperature. (h) Reading of ΔRW in pure water at different temperatures. Each continuous measurement lasted for 1 min. Calculations of (i) $\bar{\sigma}$ and (j) $\bar{S}$ using data from (h). The baseline for each ΔRW was the sensor signal obtained in pure water at 25 °C. The temperature in (a–e) was maintained at 25 °C. Samples in (f–j) were pure water.

https://doi.org/10.1021/acsnano.3c05007
ACS Nano 2023, 17, 12903–12914

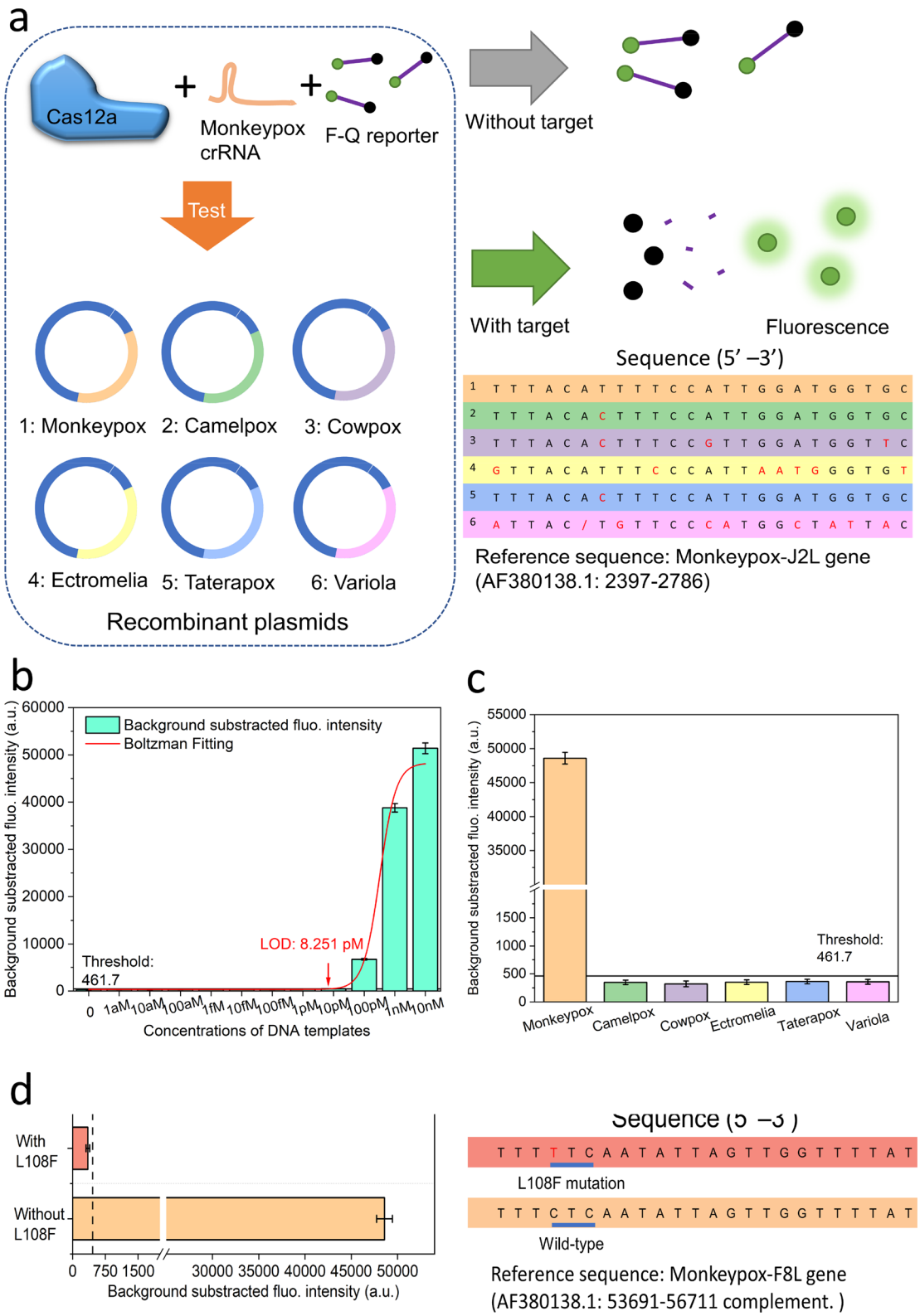

Figure 4. CRISPR/Cas12a fluorescence assay. (a) Scheme of the fluorescence assay. (b) Limit of detection (LOD) of the CRISPR/Cas12a fluorescence assay was measured by the reaction between the correctly paired crRNA and dsDNA templates at different concentrations. Specificity of the crRNA–dsDNA pairs was evaluated by cross-reactions between the (c) crRNA targeting the MPXV *F2L* gene and DNA templates of the MPXV sequence or similar gene sequences from other orthopoxviruses (brake: 2000–30 000), and (d) crRNA targeting the MPXV *F8L* gene and DNA templates of the *F8L* gene from the MPXV sequence without or with the L108F mutation.

other orthopoxviruses, including Camelpox virus, *Cowpox virus*, *Ectromelia*, *Taterapox virus*, and *Variola*, were established (Figure 4a).

The limit of detection (LOD) of the CRISPR/Cas12a fluorescence assay was measured according to the reaction between the correctly paired crRNA and dsDNA templates at

https://doi.org/10.1021/acsnano.3c05007
ACS Nano 2023, 17, 12903–12914

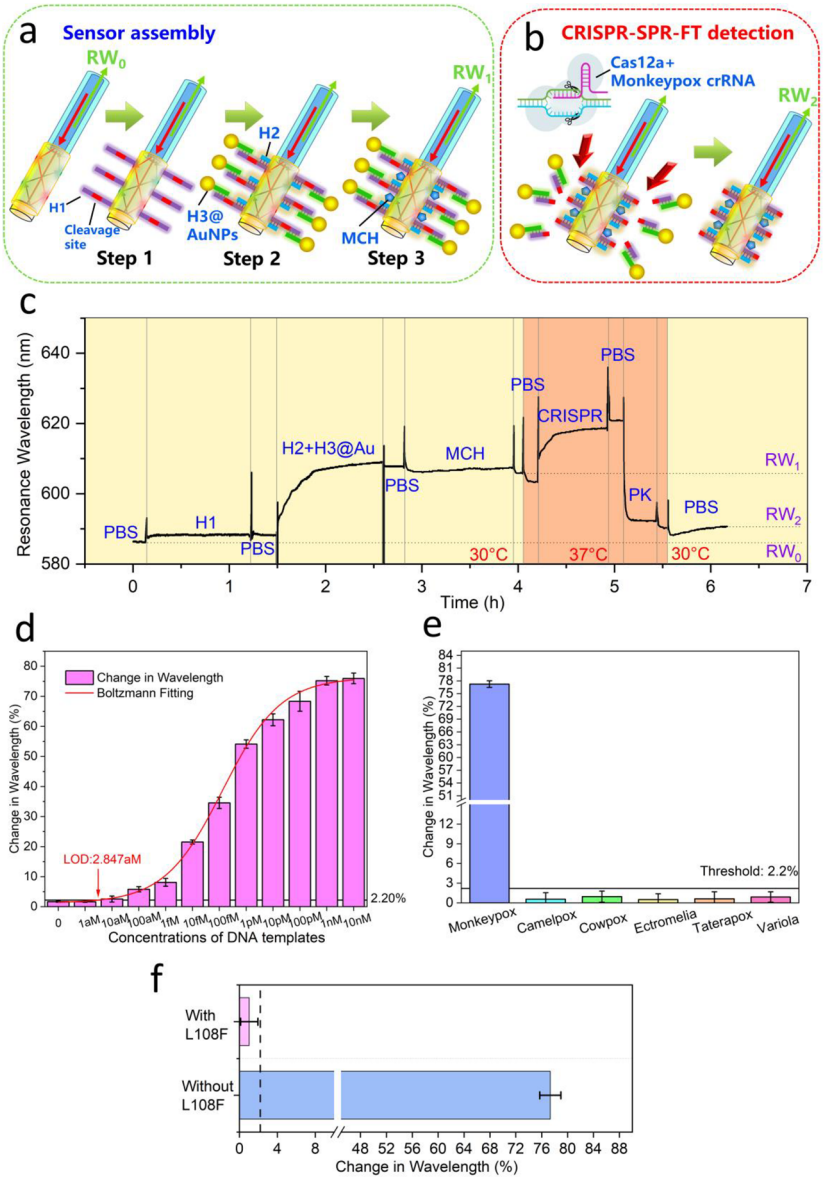

Figure 5. On-device measurement with the CRISPR-SPR-FT biosensor. (a, b) On-device workflow. (c) Full streamline of the signal. (d) Surface plasmon resonance (SPR) signal with different concentrations of the target dsDNA template. The specificity of on-device measurement was verified by cross-reaction of (e) crRNA targeting the *F2L* gene from the MPXV sequence and DNA templates of the MPXV sequence or similar gene sequences from other orthopoxviruses (brake: 15−50), and (f) crRNA targeting the *F8L* gene from the MPXV sequence and DNA templates of the *F8L* gene from the MPXV sequence without or with the L108F mutation.

different concentrations (Figure 4b). Following International Union of Pure and Applied Chemistry guidelines,[41] the threshold of the CRISPR sensing system signal was estimated as the sum of the blank measures (without the target) plus triple its standard deviation. The LOD was calculated as 8.251 pM by fitting the calibrated regression curve.

The specificity of the crRNA−dsDNA pairs was determined by cross-reactions between the crRNA targeting the MPXV sequence with the L108F mutation in the F8L gene and all dsDNA templates (10 nM). Only the correctly paired reactions were observed with strong fluorescence signals (Figure 4c,d).

Based on the above results, highly specific trans-cleavage of crRNA targeting a specific gene sequence with a single-base mutation was verified. However, DNA templates at low concentrations (<8.251 pM) could not be determined. Therefore, the CRISPR-SPR-FT biosensor was designed to improve sensitivity.

On-Device Measurement of the CRISPR-SPR-FT Biosensor. Building upon the demonstrated specificity of the crRNA target sequences, on-device measurements were conducted to further enhance sensitivity and lower the LOD of the biosensor, aiming to fulfill the requirements for detecting nonamplified samples collected directly from patients for point-of-care testing. The overall on-device workflow, encompassing both the sensor decoration process and the CRISPR-SPR-FT detection process, is depicted in Figure 5a,b. For sensor decoration, a complex reporter constructed from three ssDNA and AuNPs was assembled onto the surface of the proposed biosensor: H1, a long handle containing a sequence for trans-cleavage of activated Cas12a; H2, a short handle with a complementary sequence of part of H1; H3, another short

https://doi.org/10.1021/acsnano.3c05007
ACS Nano 2023, 17, 12903−12914

handle with a complementary sequence of the other part of H1, to which AuNPs were attached using the freezing method,[42] forming H3@AuNPs. After the phosphate-buffered saline (PBS) was equilibrated on the SPR-based fiber tip biosensor (RW_0), H1 was first immobilized onto the Au surface of the biosensor. Following a brief washing step in PBS, the biosensor was immersed in a mixture of H2 and AuNP@H3 handles. By forming DNA complexes, AuNPs were assembled onto the surface of the biosensors at a controlled distance, resulting in a significant SPR signal increase. The assembly process was verified by monitoring the successful loading of H1, H2, and H3 handles in Figure S2: A slight increase in wavelength was observed when the SH−H1 handle was loaded onto the tip, and it reached a plateau rapidly (5 min). After a brief rinse, H2, H3@AuNP, and H2+H3@AuNP handles were loaded. The H2 handle had little shift in wavelength, while the H3@AuNP handle induced an obvious signal shift (such a shift was not observed when the tips were immersed in a solution with only H3@AuNP, in the preliminary experiments). The H2+H3@AuNP handles induced an even higher change in wavelength than the H3@AuNP handle alone, and this higher part was more than that of the H2 handle alone. The AuNP modified CRISPR-SPR-FT biosensor can be dried under N2 and stored at 4 °C in the dark under nitrogen protection before use, without a significant loss of activity for one month. As shown in Figure S3, three AuNP modified CRISPR-SPR-FT biosensors were tested by immersing them in PBS and measuring the shifted wavelength of the tip, which remained higher than 90% of the original wavelength.

After being blocked with 6-mercaptohexanol mercaptoethanol (MCH), loosely adsorbed ssDNAs were detached from the Au surface. After the sensor was washed with PBS, the sensor preparation process was completed, and the corresponding SPR signal was recorded as RW1.

The CRISPR-SPR-FT detection process comprises the CRISPR reaction, Proteinase K washing, and PBS washing steps, taking a total of 1.5 h. During the CRISPR reaction process, the Cas12a protein is activated if the target DNA is present in the reaction mixture, leading to the trans-cleavage of H1 and subsequent release of AuNPs. The optimal concentrations of Cas12a and crRNA in the reaction matrix were determined in preliminary experiments (Figure S4). To avoid unspecific absorption of Cas12a onto the tips, the principle of optimization was to select the lowest concentration of Cas12a that could achieve complete trans-cleavage on the CRISPR-SPR-FT biosensors (RW_1−RW_2).

After washing the surface to remove nonspecific absorption of substances such as the Cas12a protein, the final SPR signal (RW_2) can be determined. The complete streamline of the SPR signal is displayed in Figure 5c. Notably, RW_0, RW_1, and RW_2 were obtained in a PBS background at 30 °C to minimize environmental disturbances.

We calculated the ΔWavelength as $[(RW_1 - RW_2)/(RW_1 - RW_0)] \times 100\%$ to quantify the concentration of target dsDNA templates. A greater amount of the target sequence in the reaction will activate more Cas12a, thereby cleaving more of the H1 handle within a given period. Consequently, the ΔWavelength signal reflects the concentration of the target sequences. ΔWavelength measured at different concentrations of the target dsDNA template is shown in Figure 5d. Following the same principle applied in CRISPR/Cas12a-based detection, the LOD of the CRISPR-SPR-FT biosensor was calculated to be 2.847 aM, which can detect samples with virus concentrations lower than 1.8 copies/μL without necessitating a preamplification step.

Subsequently, the specificity of the on-device measurement was verified through the cross-reaction of each crRNA and dsDNA template (Figure 5e). Correctly paired crRNA and dsDNA resulted in a significantly higher ΔWavelength (77.33 ± 1.63%) compared to any incorrectly paired groups. The specificity was cross-validated according to the results of the fluorescence assay in a manner similar to the CRISPR fluorescence assay; only the correctly paired dsDNA sample and crRNA generated strong signals (Figure 5e,f), indicating the robust specificity of the CRISPR system with enhanced gene sequence detection due to the SPR-based fiber tip biosensing.

In summary, the CRISPR-SPR-FT biosensor effectively improved the sensitivity and specificity of the CRISPR/Cas12a system for the detection of MPXV DNA. The on-device measurements demonstrated that the biosensor could detect target sequences at very low concentrations without requiring preamplification steps. This portable, sensitive, and specific platform has great potential for point-of-care testing and rapid detection of various pathogens, including those responsible for emerging infectious diseases.

Feasibility of CRISPR-SPR-FT Biosensor in Simulated Blood Specimens. Artificially inoculated pseudotyped virus in blood samples was used to practically validate the feasibility of the CRISPR-SPR-FT biosensor.[17] To further evaluate the practical application of the CRISPR-SPR-FT biosensor, we examined its performance in simulated blood specimens. First, we spiked various concentrations of the MPXV pseudovirus containing J2L and F8L genes into human blood samples, simulating a range of viral loads that could be encountered in clinical settings. To remove potential inhibitors and contaminants, a simple nucleic acid extraction method was employed. The extracted DNA was then subjected to the CRISPR-SPR-FT detection process, as described in the previous sections. As shown in Figure 6, The CRISPR-SPR-FT biosensor maintained its high sensitivity and specificity with a limit of detection of 59.5 copies/μL, which is near 98.8 aM DNA, indicating that the CRISPR-SPR-FT biosensor is still sensitive when testing a more complexed sample matrix. Above all, the CRISPR-SPR-FT biosensor displayed feasibility for detecting MPXV DNA in simulated blood specimens. These results further support the

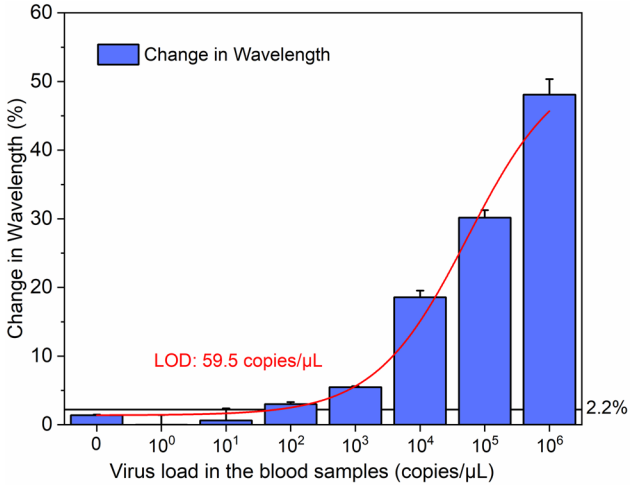

Figure 6. Sensitivity and specificity of CRISPR-SPR-FT for the detection of simulated blood specimens.

https://doi.org/10.1021/acsnano.3c05007
ACS Nano 2023, 17, 12903−12914

potential of the biosensor as a reliable, rapid, and portable platform for point-of-care testing and the detection of various pathogens in blood samples.

CONCLUSIONS

In this study, we developed a CRISPR-SPR-FT biosensor as a label-free and rapid technique for MPXV detection and mutation analysis. First, the biosensor combines the sequence-specific recognition ability of the CRISPR/Cas12a system with the high sensitivity of the SPR-based fiber tip sensor. Furthermore, the biosensor can detect MPXV DNA and the L108F mutation site without amplification steps with a limit of detection below 5 aM in plasmids and about 59.5 copies/μL in pseudovirus-spiked blood samples. Moreover, the biosensor also features a streamlined workflow and a flexible design that allows for the attachment of other nanomaterials to the reporter for an enhanced SPR signal response and multiplex gene detection. Leveraging the integrated sequence-specific recognition ability of the CRISPR/Cas system and the high sensitivity of the SPR sensor, this work demonstrates the advantages of combining the CRISPR/Cas12a system with the SPR-based fiber tip biosensor for gene detection, such as label-free, rapid, portable, sensitive, specific, programmable, and multiplex capabilities. The CRISPR-SPR-FT biosensor has great potential for clinical applications and public health surveillance in the face of emerging infectious diseases.

METHODS AND EXPERIMENTAL SECTION

Materials and Instruments. Tris(2-carboxyethyl) phosphine hydrochloride (TCEP), MCH, and ethylenediaminetetraacetic acid (all analytical grade) were purchased from Macklin Biochemical Co., Ltd. (Shanghai, China). Primer sets were synthesized by Shanghai Generay Biotech Co., Ltd. (Shanghai, China). Cas12a protein and 10× Cas12a Reaction Mix were purchased from New England Biolabs (NEB) Inc. (Ipswich, MA, USA). Other oligonucleotides, including the crRNA, MB-ssDNA reporter, and FAM-ssDNA reporter, were synthesized by Sangon Biotech (Shanghai) Co., Ltd. and purified by high-performance liquid chromatography.

CF (125 μm) and MMF (50/125 μm), as the materials of the core fiber sensor, were purchased from Sussess Prime (Taiwan, China) and Yangtze (Wuhan, China), respectively. Fiber splicer electrodes, fiber cutters (Fujikura, Tokyo, Japan), and tin foil (Rigorous, Shenzhen, China) were used to fabricate the fiber-sensing structure. A 4N-purity Au target, used as the SPR-excited material, was acquired from ZhongNuo Advanced Material (Beijing, China).

The CRISPR-SPR-FT biosensing system is mainly composed of a microspectrometer with a visible-near-infrared detection range (Ocean Optics, Orlando, FL, USA), an HL2000-12 light source (Fu Xiang, Shanghai, China), a 50/50 optical fiber splitter coupler, and a thermal control platform (Joanlab, Zhejiang, China).

A Cary Eclipse fluorescence spectrophotometer (Agilent Technologies, Palo Alto, CA, USA) was used to read the fluorescence spectra. The DNA suspension concentrations were quantified by using a NanoDrop 1000 spectrophotometer (Thermo Scientific, Waltham, MA, USA). Agarose gel electrophoresis analysis was performed using an electrophoresis analyzer (Bio-Rad, Hercules, CA, USA) and imaged with a ChemiDoc XRS system (Bio-Rad).

Fabrication of the SPR-Based Fiber Tip Biosensor. To facilitate combination with the CRISPR/Cas12a system, the optical fiber SPR biosensor was designed as a plug-in probe.[43,44] A fiber cutter was first employed to cut MMF and CF to achieve flat-end faces, and the control length of the CF was 5 mm. After aligning and splicing the flat-end faces of the MMF and CF, an MMF−CF structure was acquired using fusion splicer electrodes. The CF sensing region was wrapped in tin foil to avoid contamination from the end-face coating, and an end-face Au mirror of 300 nm was coated onto the outgoing end of the CF. After removing the tin foil, the cylinder of the CF sensing region was coated with an Au sensing film of 50 nm using a rotary coating mechanism, as reported previously.[45]

Preparation of DNA Templates. The CRISPR-SPR-FT biosensor uses the CRISPR/Cas12a system to detect specific target gene sequences. To demonstrate this ability, several recombinant pUC57 plasmids were prepared as the dsDNA templates, including regions of the *F8L* sequence in the MPXV genome with or without the L108F mutation, *Camelpox*, *Cowpox*, *Ectromelia*, *Taterapox virus*, and *Variola*, respectively. Detailed inserted sequences are listed in Table S1. After PCR amplification (primers are shown in Table S2), the concentrations of linear dsDNA products were measured using a NanoDrop spectrophotometer (ThermoFisher Scientific) and stored at −80 °C until use.

Verification of the Specificity of the CRISPR/Cas12a Assay. There are two components of Cas12a crRNAs: the universal scaffold region (UAAUUUCUA CUAAGUGUAGAU) for Cas12a protein recognition and binding and a customized region added to the 3′ end of the scaffold that provides specificity to the target sequences (the same sequence as the region following a TTTV PAM sequence). The design principle was consistent with the "CRISPR-SHERLOCK" method published by Zhang et al.[46] The crRNA targeting the L108F mutation of the MPXV *F8L* gene was provided by Sangon Biotech (Shanghai) Co., Ltd. (see Table S1 for the crRNA sequence).

The specificity of crRNAs for different DNA templates was validated by using the CRISPR/Cas12a assay. In 10 μL volumes, 100 nM Cas12a (NEB), 100 nM crRNA, 1× NEB 2.1 buffer (NEB), 500 nM ssDNA fluorescent quenched reporter (5′ 6-FAM/TTATT/BHQ-1 3′, Sangon), and different concentrations of target dsDNA sequences diluted in RNase-free water were used. Reactions were incubated at 37 °C for 30 min, and real-time fluorescence was measured using a BioTek NEO HTS plate reader (BioTek Instruments, Winooski, VT, USA) with readings every 2 min (excitation: 485 nm; emission: 528 nm). The cis-cleavage of the sequences was further verified by electrophoresis on a 2% agarose gel at 120 V for 30 min (Figure S1).

Sensor Assembly for CRISPR-SPR-FT Biosensing. The H3 ssDNA handle (Table S1) assembled reporter was used to decorate the SPR-based fiber-tip biosensor. First, 100 μM H3 DNA solution was mixed with 10 mM TECP (v/v = 1/1) for 1 h before being added to the AuNP solutions (15 nm, obtained from Nanoeast BioTech, Nanjing, China) (2.5 nM AnNP with 1.25 μM DNA). After a brief vortex, the H3@AuNPs mixture was placed at −20 °C for a least 2 h and the solution was thawed at room temperature (25 °C). Finally, the mixture was centrifuged at 12 000 rpm for 20 min, and the supernatant was removed. The pellet was washed three times to remove free DNA. The conjugate (H3@AuNPs) was redispersed in PBS for further use.

To decorate H3@AuNPs on the sensor surface, the following three main steps were conducted at 30 °C: (1) H1 ssDNA handle immobilization on the sensor surface, (2) H2 and H3@AuNPs hybridization with the H1 ssDNA handle, and (3) MCH blocking. First, the H1 ssDNA handle functionalized with S−S at the 5′ end (Table S1) was activated with 10 mM TCEP for 1 h before being diluted to 5 μM for sensor assembly. After washing with PBS, the H1-decorated sensor was immersed in a mixture of H2 (5 μM) and H3@AuNPs (described above) for reporter complex assembly. A significant SPR signal increase was observed at this step owing to the massive surface load increase due to the AuNPs. Finally, the sensor was immersed in the MCH (1 mM) solution to remove loosely adsorbed DNAs. After a brief washing step with PBS buffer, the CRISPR-SPR-FT biosensor was completed and ready for CRISPR detection.

Target DNA Detection by CRISPR-SPR-FT Biosensing. The detection process was carried out at 30−37 °C. The SPR-CRISPR measurements were performed at 30 °C because, although this temperature was not optimal for the activity of Cas12a protein, we need to consider maintaining the stability of the bond (−SH) connecting ssDNA reporter and Au surface, which can be severely influenced at a relatively high temperature (40 °C or higher). After brief stabilization in PBS buffer, the CRISPR-SPR-FT biosensor was inserted into the samples mixed with the CRISPR reaction solution (100 nM Cas12a, 100 nM crRNA, 1× NEB 2.1 buffer, and target dsDNA

https://doi.org/10.1021/acsnano.3c05007
ACS Nano 2023, 17, 12903−12914

sequences at desired concentrations), and the concentration of Cas12a and crRNA in the reaction matrix was optimized in preliminary experiments (Figure S4). After approximately 40 min of incubation, the biosensor was briefly immersed in PBS buffer and then inserted into Proteinase K (1:1000) solution to remove the nonspecific binding of Cas12a protein on the sensor surface. Finally, the biosensor was briefly washed in PBS buffer and re-equilibrated to 30 °C to record the final SPR signal for quantitative analysis.

Evaluating CRISPR-SPR-FT Biosensor Performance in Simulated Blood Specimens. The MPXV pseudotyped virus, incorporating both the J2L and F8L genes, was custom-designed and produced by Sangon Biotech Co., Ltd. The procedure for generating the pseudotype virus consisted of the following steps.

Target Sequence Design and Cloning. A specific 900-bp target sequence, encompassing the J2L and F8L genes of MPXV, was designed and subsequently cloned into *Escherichia coli* BJ5183 competent cells, which also contained the adenovirus vector pAdeasy-1, allowing for seamless recombination.

Preparation of the Simulated Blood Specimens. Human blood samples were collected from healthy donors, and informed consent was obtained. The MPXV pseudotype virus was spiked into the blood samples to create a range of viral loads that might be encountered in clinical settings. The virus concentrations used in blood samples varied from 1 to 1×10^6 copies/μL, which almost equals 1.66 aM−1.66 pM DNA concentrations.

Nucleic Acid Extraction from Blood Samples. To remove potential inhibitors and contaminants from the blood samples, a simple nucleic acid extraction method was employed. The blood samples were centrifuged, and the plasma was separated. The MPXV target DNA was extracted from the plasma using a commercial DNA extraction kit, following the manufacturer's instructions.

CRISPR-SPR-FT Biosensor Detection Process. The extracted DNA samples were subjected to the CRISPR-SPR-FT detection process, as described in the previous sections of the manuscript. The CRISPR/Cas12a-crRNA complexes were prepared, and the target DNA was incubated with the complexes. The trans-cleavage reaction was initiated by adding the ssDNA reporter to the reaction mix. The SPR fiber tip biosensor was then exposed to the reaction solution, and the shift in wavelength was recorded for further analysis.

Statistical Analysis. All measurements were performed in triplicate (n = 3), and the data are presented as mean ± standard deviation. Correlations were performed using linear regression to determine the goodness of fit (Pearson's correlation coefficient, R2). For intersample comparisons, multiple pairs of samples were analyzed using a two-tailed t test, and the resulting P-values were adjusted for multiple hypothesis testing using the Bonferroni correction. $P < 0.05$ was used as a threshold to indicate a statistically significant difference. All statistical analyses were performed using OriginPro software (v.2022).

ASSOCIATED CONTENT

Data Availability Statement

The data that support the findings of this study are available from the corresponding author, upon reasonable request.

Supporting Information

The Supporting Information is available free of charge at https://pubs.acs.org/doi/10.1021/acsnano.3c05007.

Figure S1, verification of cis-cleavage; Figure S2, comparison of H2, H3@Au, or H2+H3@Au signal; Figure S3, duration of the biosensor; Figure S4, optimization of concentration of Cas12a; Figure S5, optimization of concentration of H1 handle; Table S1, sequences of primers, crRNAs, and reporters; Table S2, sequences of viruses (PDF)

AUTHOR INFORMATION

Corresponding Authors

Jingfeng Li − *College of Physics and Optoelectronic Engineering, Shenzhen University, Shenzhen 518060, People's Republic of China; Shenzhen International Institute for Biomedical Research, Shenzhen, Guangdong 518110, People's Republic of China*; Email: ljfeng0623@163.com

Zhongjian Xie − *Institute of Pediatrics, Shenzhen Children's Hospital, Shenzhen, Guangdong 518038, People's Republic of China*; Email: xiezj2022@sustech.edu.cn

Li Xuejin − *College of Physics and Optoelectronic Engineering, Shenzhen University, Shenzhen 518060, People's Republic of China; Shenzhen Key Laboratory of Sensor Technology, Shenzhen 518060, People's Republic of China; The Chinese University of Hong Kong, Shenzhen, Guangdong 518060, People's Republic of China*; Email: lixuejin@szu.edu.cn

Han Zhang − *College of Physics and Optoelectronic Engineering and International Collaborative Laboratory of 2D, Materials for Optoelectronics Science and Technology of Ministry of Education, Institute of Microscale Optoelectronics, Shenzhen University, Shenzhen 518060, People's Republic of China*; orcid.org/0000-0002-0166-1973; Email: hzhang@szu.edu.cn

Authors

Yuzhi Chen − *College of Physics and Optoelectronic Engineering, Shenzhen University, Shenzhen 518060, People's Republic of China; Shenzhen Key Laboratory of Sensor Technology, Shenzhen 518060, People's Republic of China*; orcid.org/0000-0002-5975-3053

Zhi Chen − *College of Physics and Optoelectronic Engineering, Shenzhen University, Shenzhen 518060, People's Republic of China; The Sixth Affiliated Hospital of Guangzhou Medical University, Qingyuan People's Hospital, Qingyuan, Guangdong 511518, People's Republic of China; Shenzhen International Institute for Biomedical Research, Shenzhen, Guangdong 518110, People's Republic of China*; orcid.org/0000-0002-7624-3143

Tianzhong Li − *College of Physics and Optoelectronic Engineering, Shenzhen University, Shenzhen 518060, People's Republic of China*

Meng Qiu − *College of Chemistry and Chemical Engineering, Key Laboratory of Marine Chemistry Theory and Technology, Ministry of Education, Ocean University of China, Qingdao, Shandong 266100, People's Republic of China*; orcid.org/0000-0002-3312-4873

Jinghan Zhang − *College of Physics and Optoelectronic Engineering, Shenzhen University, Shenzhen 518060, People's Republic of China; Shenzhen Key Laboratory of Sensor Technology, Shenzhen 518060, People's Republic of China; The Chinese University of Hong Kong, Shenzhen, Guangdong 518060, People's Republic of China*

Yan Wang − *College of Physics and Optoelectronic Engineering, Shenzhen University, Shenzhen 518060, People's Republic of China; Shenzhen Key Laboratory of Sensor Technology, Shenzhen 518060, People's Republic of China*

Wu Yuan − *Department of Biomedical Engineering, The Chinese University of Hong Kong, Hong Kong 999077, People's Republic of China*; orcid.org/0000-0001-9405-519X

Aaron Ho-Pui Ho − *Department of Biomedical Engineering, The Chinese University of Hong Kong, Hong Kong 999077, People's Republic of China*; orcid.org/0000-0001-5001-5911

https://doi.org/10.1021/acsnano.3c05007
ACS Nano 2023, 17, 12903−12914

Omar Al-Hartomy − *Department of Physics, Faculty of Science, King Abdulaziz University, Jeddah 21589, Saudi Arabia*
Swelm Wageh − *Department of Physics, Faculty of Science, King Abdulaziz University, Jeddah 21589, Saudi Arabia;* orcid.org/0000-0002-9494-4568
Abdullah G. Al-Sehemi − *Research Center for Advanced Materials Science (RCAMS) and Department of Chemistry, College of Science, King Khalid University, Abha 61413, Saudi Arabia;* orcid.org/0000-0002-6793-3038
Xin Shi − *China Medical University, Shenyang, Liaoning 110001, People's Republic of China; School of Mathematics and Information Science, Shandong Technology and Business University, Yantai, Shandong 264005, People's Republic of China; Manchester Metropolitan University (MMU), Operations, Technology, Events and Hospitality Management, Business School, Manchester M15 6BH, United Kingdom*

Complete contact information is available at: https://pubs.acs.org/10.1021/acsnano.3c05007

Author Contributions

#Yuzhi Chen and Zhi Chen contributed equally to this work and should be considered cofirst authors. **Yuzhi Chen**: Conceptualization, Data Curation, Formal analysis, Investigation, Methodology, Software, Validation, Visualization, Writing−original draft, and Writing−review and editing; **Zhi Chen**: Conceptualization, Data Curation, Formal analysis, Investigation, Methodology, Software, Validation, Visualization, Writing−original draft, and Writing−review and editing; **Tianzhong Li**: Investigation and Software; **Meng Qiu**: Investigation and Software; **Jinghan Zhang**: Investigation and Software; **Yan Wang**: Investigation and Software; **Wu Yuan**: Investigation; **Aaron Ho-Pui Ho**: Investigation; **Omar Al-Hartomy**: Investigation; **Swelm Wageh**: Investigation; **Abdullah G. Al-Sehemi**: Investigation; **Xin Shi**: Funding acquisition; **Jingfeng Li**: Data Curation, Formal analysis, Investigation, Software, Visualization, Methodology, Supervision, and Writing−review and editing; **Zhongjian Xie**: Supervision and Funding acquisition; **Li Xuejin**: Supervision and Funding acquisition; **Han Zhang**: Supervision, Project administration, and Funding acquisition.

Notes

The authors declare no competing financial interest.

ACKNOWLEDGMENTS

The authors are grateful for the financial support from the National Natural Science Foundation of China (U21A20511, 81870337, U1813207, 12274197), Key Projects (B) of the Stability Support Program for Shenzhen Higher Education Institutions (No. 20220810151419001), Science and Technology Innovation Leading Talents Program of Guangdong Province (No. 2019TX05C343), Department of Education of Guangdong Province (No. 2022ZDZX1023), Basic and Applied Basic Research Foundation of Guangdong Province-Regional Joint Fund-Key Projects (2022B1515120012 and 2019B1515120043), Central Military Commission Science and Technology Committee Project (2022-JCJQ-JJ-0886), Science and Technology Innovation Commission of Shenzhen (JCYJ20220818102618040, JCYJ20200109105608771, KCXFZ20201221173413038, and KCXFZ20211020163814021), Project supported by State Key Laboratory of Luminescence and Applications (SKLA-2020-03), National Taipei University of Technology-Shenzhen University Joint Research Program (2021008), Innovation Team Project of the Department of Education of Guangdong Province (No. 2018KCXTD026), Plan on enhancing scientific research in Guangzhou Medical University (GZMU-SH-001), Guangdong Medical Science and Technology Research Fund (A2023421), Immersion Technology and Evaluation Shandong Engineering Research Center (2022), Immersive Smart Devices for Healthcare System R&D and Industrial Application Innovation Platform (2022), National key research and development program of China (2022YFB3207200), Natural Science Foundation of Guangdong Province (2021A1515010717), Guangdong Scientific and Technological Project (2019B1515120043, 2020A1515010612, 2021A1515220109, 2022B1515020093), Stabilization Support Program for Higher Education Institutions of Shenzhen (No. 20200812115548001), Shenzhen Bay Laboratory Open Fund Project (No. SZBL2021080601012), and High-end Talent Scientific Research Startup Project (No. 827-000636). The authors acknowledge the support and funding of King Khalid University through Research Center for Advanced Materials Science (RCAMS) under grant No. RCAMS/KKU/006/21. The Deanship of Scientific Research (DSR) at King Abdulaziz University, Jeddah, Saudi Arabia, has funded this project under grant No. FP-158-43. Authors also acknowledge the support from Instrumental Analysis Center of Shenzhen University (Xili Campus).

REFERENCES

(1) Kumar, N.; Acharya, A.; Gendelman, H. E.; Byrareddy, S. N. The 2022 outbreak and the pathobiology of the monkeypox virus. *J. Autoimmun* **2022**, *131*, 102855.
(2) Guarner, J.; Del Rio, C.; Malani, P. N. Monkeypox in 2022-What Clinicians Need to Know. *JAMA* **2022**, *328* (2), 139−140.
(3) Gigante, C. M.; Korber, B.; Seabolt, M. H.; Wilkins, K.; Davidson, W.; Rao, A. K.; Zhao, H.; Smith, T. G.; Hughes, C. M.; Minhaj, F.; Waltenburg, M. A.; Theiler, J.; Smole, S.; Gallagher, G. R.; Blythe, D.; Myers, R.; Schulte, J.; Stringer, J.; Lee, P.; Mendoza, R. M.; Griffin-Thomas, L. A.; Crain, J.; Murray, J.; Atkinson, A.; Gonzalez, A. H.; Nash, J.; Batra, D.; Damon, I.; McQuiston, J.; Hutson, C. L.; McCollum, A. M.; Li, Y. Multiple lineages of monkeypox virus detected in the United States, 2021−2022. *Science* **2022**, *378*, 560.
(4) Luna, N.; Ramirez, A. L.; Munoz, M.; Ballesteros, N.; Patino, L. H.; Castaneda, S. A.; Bonilla-Aldana, D. K.; Paniz-Mondolfi, A.; Ramirez, J. D. Phylogenomic analysis of the monkeypox virus (MPXV) 2022 outbreak: Emergence of a novel viral lineage? *Travel Med. Infect Dis* **2022**, *49*, 102402.
(5) Siegrist, E. A.; Sassine, J. Antivirals with Activity Against Monkeypox: A Clinically Oriented Review. *Clin Infect Dis* **2023**, *76*, 155.
(6) Schnierle, B. S. Monkeypox Goes North: Ongoing Worldwide Monkeypox Infections in Humans. *Viruses* **2022**, *14* (9), 1874.
(7) Kannan, S. R.; Sachdev, S.; Reddy, A. S.; Kandasamy, S. L.; Byrareddy, S. N.; Lorson, C. L.; Singh, K. Mutations in the monkeypox virus replication complex: Potential contributing factors to the 2022 outbreak. *J. Autoimmun* **2022**, *133*, 102928.
(8) Doudna, J. A.; Charpentier, E. Genome editing. The new frontier of genome engineering with CRISPR-Cas9. *Science* **2014**, *346* (6213), 1258096.
(9) Zetsche, B.; Gootenberg, J. S.; Abudayyeh, O. O.; Slaymaker, I. M.; Makarova, K. S.; Essletzbichler, P.; Volz, S. E.; Joung, J.; van der Oost, J.; Regev, A.; Koonin, E. V.; Zhang, F. Cpf1 is a single RNA-guided endonuclease of a class 2 CRISPR-Cas system. *Cell* **2015**, *163* (3), 759−71.
(10) Abudayyeh, O. O.; Gootenberg, J. S.; Konermann, S.; Joung, J.; Slaymaker, I. M.; Cox, D. B.; Shmakov, S.; Makarova, K. S.; Semenova, E.; Minakhin, L.; Severinov, K.; Regev, A.; Lander, E. S.; Koonin, E. V.;

Zhang, F. C2c2 is a single-component programmable RNA-guided RNA-targeting CRISPR effector. *Science* **2016**, *353* (6299), aaf5573.
(11) Li, Y.; Zeng, R.; Wang, W.; Xu, J.; Gong, H.; Li, L.; Li, M.; Tang, D. Size-Controlled Engineering Photoelectrochemical Biosensor for Human Papillomavirus-16 Based on CRISPR-Cas12a-Induced Disassembly of Z-Scheme Heterojunctions. *ACS Sens* **2022**, *7* (5), 1593−1601.
(12) Gong, H.; Wu, Y.; Zeng, R.; Zeng, Y.; Liu, X.; Tang, D. CRISPR/Cas12a-mediated liposome-amplified strategy for the photoelectrochemical detection of nucleic acid. *Chem. Commun. (Camb)* **2021**, *57* (71), 8977−8980.
(13) Zeng, R.; Xu, J.; Lu, L.; Lin, Q.; Huang, X.; Huang, L.; Li, M.; Tang, D. Photoelectrochemical bioanalysis of microRNA on yolk-in-shell Au@CdS based on the catalytic hairpin assembly-mediated CRISPR-Cas12a system. *Chem. Commun. (Camb)* **2022**, *58* (54), 7562−7565.
(14) Broughton, J. P.; Deng, X.; Yu, G.; Fasching, C. L.; Servellita, V.; Singh, J.; Miao, X.; Streithorst, J. A.; Granados, A.; Sotomayor-Gonzalez, A.; Zorn, K.; Gopez, A.; Hsu, E.; Gu, W.; Miller, S.; Pan, C. Y.; Guevara, H.; Wadford, D. A.; Chen, J. S.; Chiu, C. Y. CRISPR-Cas12-based detection of SARS-CoV-2. *Nat. Biotechnol.* **2020**, *38* (7), 870−874.
(15) Tian, T.; Shu, B.; Jiang, Y.; Ye, M.; Liu, L.; Guo, Z.; Han, Z.; Wang, Z.; Zhou, X. An Ultralocalized Cas13a Assay Enables Universal and Nucleic Acid Amplification-Free Single-Molecule RNA Diagnostics. *ACS Nano* **2021**, *15* (1), 1167−1178.
(16) Chen, Y.; Fan, L.; Deng, W.; Lin, Q.; Chen, L.; Ren, T. Highly Pathogenic Avian Influenza outbreaks amongst bird populations in Europe - a view from China. *J. Infect* **2022**, *85* (6), 702−769.
(17) Zhou, J.; Xiao, F.; Fu, J.; Jia, N.; Huang, X.; Sun, C.; Liu, C.; Huan, H.; Wang, Y. Rapid detection of monkeypox virus by multiple cross displacement amplification combined with nanoparticle-based biosensor platform. *J. Med. Virol* **2023**, *95* (2), e28479.
(18) Chen, Q.; Gul, I.; Liu, C.; Lei, Z.; Li, X.; Raheem, M. A.; He, Q.; Haihui, Z.; Leeansyah, E.; Zhang, C. Y.; Pandey, V.; Du, K.; Qin, P. CRISPR-Cas12-based field-deployable system for rapid detection of synthetic DNA sequence of the monkeypox virus genome. *J. Med. Virol* **2023**, *95* (1), e28385.
(19) Zeng, R.; Wang, W.; Chen, M.; Wan, Q.; Wang, C.; Knopp, D.; Tang, D. CRISPR-Cas12a-driven MXene-PEDOT:PSS piezoresistive wireless biosensor. *Nano Energy* **2021**, *82*, 105711.
(20) Zeng, R.; Gong, H.; Li, Y.; Li, Y.; Lin, W.; Tang, D.; Knopp, D. CRISPR-Cas12a-Derived Photoelectrochemical Biosensor for Point-Of-Care Diagnosis of Nucleic Acid. *Anal. Chem.* **2022**, *94* (20), 7442−7448.
(21) Chen, Z.; Li, J.; Li, T.; Fan, T.; Meng, C.; Li, C.; Kang, J.; Chai, L.; Hao, Y.; Tang, Y.; Al-Hartomy, O. A.; Wageh, S.; Al-Sehemi, A. G.; Luo, Z.; Yu, J.; Shao, Y.; Li, D.; Feng, S.; Liu, W. J.; He, Y.; Ma, X.; Xie, Z.; Zhang, H. A CRISPR/Cas12a-empowered surface plasmon resonance platform for rapid and specific diagnosis of the Omicron variant of SARS-CoV-2. *Natl. Sci. Rev.* **2022**, *9* (8), nwac104.
(22) Xin, H.; Namgung, B.; Lee, L. P. Nanoplasmonic optical antennas for life sciences and medicine. *Nat. Rev. Mater.* **2018**, *3* (8), 228−243.
(23) Xin, H.; Sim, W. J.; Namgung, B.; Choi, Y.; Li, B.; Lee, L. P. Quantum biological tunnel junction for electron transfer imaging in live cells. *Nat. Commun.* **2019**, *10* (1), 3245.
(24) Loganathan, S. K.; Schleicher, K.; Malik, A.; Quevedo, R.; Langille, E.; Teng, K.; Oh, R. H.; Rathod, B.; Tsai, R.; Samavarchi-Tehrani, P.; Pugh, T. J.; Gingras, A. C.; Schramek, D. Rare driver mutations in head and neck squamous cell carcinomas converge on NOTCH signaling. *Science* **2020**, *367* (6483), 1264−1269.
(25) Willemsen-Seegers, N.; Uitdehaag, J. C. M.; Prinsen, M. B. W.; de Vetter, J. R. F.; de Man, J.; Sawa, M.; Kawase, Y.; Buijsman, R. C.; Zaman, G. J. R. Compound Selectivity and Target Residence Time of Kinase Inhibitors Studied with Surface Plasmon Resonance. *J. Mol. Biol.* **2017**, *429* (4), 574−586.
(26) Dai, Y.; Chiu, L. Y.; Sui, Y.; Dai, Q.; Penumutchu, S.; Jain, N.; Dai, L.; Zorman, C. A.; Tolbert, B. S.; Sankaran, R. M.; Liu, C. C. Nanoparticle based simple electrochemical biosensor platform for profiling of protein-nucleic acid interactions. *Talanta* **2019**, *195*, 46−54.
(27) Rath, P. P.; Anand, G.; Agarwal, S. Surface Plasmon Resonance Analysis of the Protein-protein Binding Specificity Using Autolab ESPIRIT. *Bio Protoc* **2020**, *10* (4), e3519.
(28) Hofer, C. T.; Di Lella, S.; Dahmani, I.; Jungnick, N.; Bordag, N.; Bobone, S.; Huang, Q.; Keller, S.; Herrmann, A.; Chiantia, S. Structural determinants of the interaction between influenza A virus matrix protein M1 and lipid membranes. *Biochim Biophys Acta Biomembr* **2019**, *1861* (6), 1123−1134.
(29) Xue, T.; Liang, W.; Li, Y.; Sun, Y.; Xiang, Y.; Zhang, Y.; Dai, Z.; Duo, Y.; Wu, L.; Qi, K.; Shivananju, B. N.; Zhang, L.; Cui, X.; Zhang, H.; Bao, Q. Ultrasensitive detection of miRNA with an antimonene-based surface plasmon resonance sensor. *Nat. Commun.* **2019**, *10* (1), 28.
(30) Zheng, F.; Chen, Z.; Li, J.; Wu, R.; Zhang, B.; Nie, G.; Xie, Z.; Zhang, H. A Highly Sensitive CRISPR-Empowered Surface Plasmon Resonance Sensor for Diagnosis of Inherited Diseases with Femtomolar-Level Real-Time Quantification. *Adv. Sci. (Weinh)* **2022**, *9* (14), 2105231.
(31) Hua, Y.; Wang, R.; Li, D. A Fiber-Based SPR Aptasensor for the In Vitro Detection of Inflammation Biomarkers. *Micromachines (Basel)* **2022**, *13* (7), 1036.
(32) Zhang, J.; Mai, X.; Hong, X.; Chen, Y.; Li, X. Optical fiber SPR biosensor with a solid-phase enzymatic reaction device for glucose detection. *Sens. Actuators, B* **2022**, *366*, 131984.
(33) Zhou, S.; Li, X.; Zhang, J.; Yuan, H.; Hong, X.; Chen, Y. Dual-fiber optic bioprobe system for triglyceride detection using surface plasmon resonance sensing and lipase-immobilized magnetic bead hydrolysis. *Biosens Bioelectron* **2022**, *196*, 113723.
(34) Mai, Z.; Zhang, J.; Chen, Y.; Wang, J.; Hong, X.; Su, Q.; Li, X. A disposable fiber optic SPR probe for immunoassay. *Biosens Bioelectron* **2019**, *144*, 111621.
(35) Liu, Y.; Peng, W. Fiber-Optic Surface Plasmon Resonance Sensors and Biochemical Applications: A Review. *Journal of Lightwave Technology* **2021**, *39* (12), 3781−3791.
(36) Qi, M.; Zhang, N. M. Y.; Li, K.; Tjin, S. C.; Wei, L. Hybrid Plasmonic Fiber-Optic Sensors. *Sensors (Basel)* **2020**, *20* (11), 3266.
(37) Zhuang, J.; Lai, W.; Xu, M.; Zhou, Q.; Tang, D. Plasmonic AuNP/g-C3N4 Nanohybrid-based Photoelectrochemical Sensing Platform for Ultrasensitive Monitoring of Polynucleotide Kinase Activity Accompanying DNAzyme-Catalyzed Precipitation Amplification. *ACS Appl. Mater. Interfaces* **2015**, *7* (15), 8330−8.
(38) Cai, G.; Yu, Z.; Ren, R.; Tang, D. Exciton-Plasmon Interaction between AuNPs/Graphene Nanohybrids and CdS Quantum Dots/TiO(2) for Photoelectrochemical Aptasensing of Prostate-Specific Antigen. *ACS Sens* **2018**, *3* (3), 632−639.
(39) Chen, Y.; Ge, Y.; Huang, W.; Li, Z.; Wu, L.; Zhang, H.; Li, X. Refractive Index Sensors Based on Ti3C2Tx MXene Fibers. *Acs Applied Nano Materials* **2020**, *3* (1), 303−311.
(40) Liu, L.; Zhang, X.; Zhu, Q.; Li, K.; Lu, Y.; Zhou, X.; Guo, T. Ultrasensitive detection of endocrine disruptors via superfine plasmonic spectral combs. *Light Sci. Appl.* **2021**, *10* (1), 181.
(41) Qiu, G.; Gai, Z.; Tao, Y.; Schmitt, J.; Kullak-Ublick, G. A.; Wang, J. Dual-Functional Plasmonic Photothermal Biosensors for Highly Accurate Severe Acute Respiratory Syndrome Coronavirus 2 Detection. *ACS Nano* **2020**, *14* (5), 5268−5277.
(42) Liu, B.; Liu, J. Freezing Directed Construction of Bio/Nano Interfaces: Reagentless Conjugation, Denser Spherical Nucleic Acids, and Better Nanoflares. *J. Am. Chem. Soc.* **2017**, *139* (28), 9471−9474.
(43) Zhao, Y.; Tong, R. J.; Xia, F.; Peng, Y. Current status of optical fiber biosensor based on surface plasmon resonance. *Biosens Bioelectron* **2019**, *142*, 111505.
(44) Zhang, S.; Han, B.; Zhang, Y. n.; Liu, Y.; Zheng, W.; Zhao, Y. Multichannel Fiber Optic SPR Sensors: Realization Methods, Application Status, and Future Prospects. *Laser & Photonics Reviews* **2022**, *16* (8), 2200009.

https://doi.org/10.1021/acsnano.3c05007
ACS Nano 2023, 17, 12903−12914

(45) Chen, Y.; Fang, L.; Yi, D.; Li, X.; Hong, X. Thermo-Optic Property Measurement Using Surface Plasmon Resonance-Based Fiber Optic Sensor. *IEEE Sensors Journal* **2020**, *20* (19), 11357−11363.
(46) Kellner, M. J.; Koob, J. G.; Gootenberg, J. S.; Abudayyeh, O. O.; Zhang, F. SHERLOCK: nucleic acid detection with CRISPR nucleases. *Nat. Protoc* **2019**, *14* (10), 2986−3012.

https://doi.org/10.1021/acsnano.3c05007
ACS Nano 2023, 17, 12903−12914